

Can antiferromagnetism and superconductivity coexist in the high-field paramagnetic superconductor Nd(O,F)FeAs?

C. Tarantini¹, A. Gurevich¹, D.C. Larbalestier¹, Z.A. Ren², X.L. Dong², W. Lu², Z.X. Zhao².
¹*National High Magnetic Field Laboratory, Florida State University, Tallahassee, Florida, 32310 USA,*
²*National Laboratory for Superconductivity, Institute of Physics, and Beijing National Laboratory for Condensed Matter Physics, Chinese Academy of Sciences, P.O. Box 603, Beijing 100190, P.R. China.*

(Dated: February 10, 2022)

We present measurements of the temperature and field dependencies of the magnetization $M(T, H)$ of Nd(O_{0.89}F_{0.11})FeAs at fields up to 33T, which show that superconductivity with the critical temperature $T_c \approx 51$ K cannot coexist with antiferromagnetic ordering. Although $M(T, H)$ at $55 < T < 140$ K exhibits a clear Curie-Weiss temperature dependence corresponding to the Neel temperature $T_N \approx 11 - 12$ K, the behavior of $M(T, H)$ below T_c is only consistent with either paramagnetism of weakly interacting magnetic moments or a spin glass state. We suggest that the anomalous magnetic behavior of an unusual high-field paramagnetic superconductor Nd(O_{1-x}F_x)FeAs is mostly determined by the magnetic Nd ions.

PACS numbers: **74.20.De**, **74.20.Hi**, **74.60.-w**

The recently discovered superconductivity in the family of doped oxypnictides [1] exhibits an unusual coexistence of the rather high critical temperature $T_c \simeq 26 - 57$ K with strong antiferromagnetic (AF) correlations and apparent magnetic ordering. Indeed, neutron [2, 3], μSR [4, 5], NMR [6, 7] and Mossbauer [8, 9] measurements have revealed complex magnetic structures including a spin density wave AF instability at $T_N \simeq 140 - 150$ K accompanied by the resistivity drop and monoclinic distortions of the tetragonal lattice of the parent semimetal compound [10]. Doping with F or O reduces T_N and seemingly eliminates manifestations of the AF ordering in the temperature dependence of the resistivity $\rho(T)$ in oxypnictides with the optimum T_c [11, 12]. This behavior poses a fundamental question if the AF ordering is merely a consequence of the nesting of the Fermi surface in the parent semimetal or it does play a major role in superconductivity. Recent theoretical models have proposed that magnetic correlations are instrumental for the unconventional superconductivity in oxypnictides [14, 15, 16, 17, 18], which may also be important for understanding their extremely high upper critical fields H_{c2} [19, 20].

In this Letter we address the specific form in which the magnetic correlations manifest themselves both in the normal and superconducting state of the Nd(O_{1-x}F_x)FeAs using high magnetic fields H up to 33T capable of destroying any global AF state with $T_N < \mu_B H / k_B \simeq 22$ K, where μ_B is the Bohr magneton. Our measurements of the magnetization $M(T, H)$ in a wide range of fields $0 < H < 33$ T and temperatures $5 < T < 140$ K have shown a strong paramagnetic contribution in $M(T, H)$ both at $T > T_c$ and $T < T_c$. In the normal state $M(T)$ exhibits a clear Curie-Weiss temperature dependence with an apparent Neel temperature $T_N \simeq 11 - 12$ K, which might sug-

gest a coexistence of superconductivity and antiferromagnetism. However, our data at $T < T_c$ show instead that $M(T, H)$ in the superconducting state is inconsistent with a long-range AF ordering, indicating that superconductivity effectively cuts off the AF interaction between magnetic moments evident at $T > T_c$. We suggest that Nd(O_{1-x}F_x)FeAs may be regarded as a *paramagnetic* superconductor with unusual magnetic behavior different not only from conventional superconductors but also from La(O_{1-x}F_x)FeAs oxypnictides. This difference may result from a large magnetic moment $\mu = 3.62\mu_B$ of a free Nd³⁺ ion ($\mu = 3.58\mu_B$ for Pr³⁺), as compared to $\mu = 0$ for La³⁺ and $\mu = 0.8\mu_B$ for Sm³⁺ [21]. Thus, $m(T, H)$ of Nd(O,F)FeAs is mostly dominated by the Curie-Weiss behavior of Nd³⁺, while contributions from Fe³⁺ with $\mu = 0.25 - 0.35\mu_B$ [2, 3] and temperature-independent van-Vleck and Pauli paramagnetism become negligible.

The Nd(O_{0.89}F_{0.11})FeAs polycrystalline samples were made as described in Ref. [13]. The sample with approximate dimensions of $1.4 \times 1 \times 0.5$ mm³, volume $V \approx 0.7$ mm³ and weight ≈ 4.5 mg had $\rho(T_c) \approx 0.53$ m Ω cm, $T_c \approx 51$ K, and about 90% of the theoretical density, 7.213 g/cm³. The magnetic susceptibility $\chi(T, H)$ and magnetic moment $M(T, H)V$ were measured by SQUID magnetometer, Vibrating Sample Magnetometer (VSM) in a 14T superconducting magnet and a resistive 33T magnet at NHMFL. Shown in Figs. 1 and 2 are the zero field cooled (ZFC) and field cooled (FC) $M(T)$ curves, which change radically upon increasing field. For $H = 10$ mT, $M(T)$ exhibits a standard superconducting behavior with the diamagnetic onset close to T_c . However, increasing field to a rather modest value of 0.5T (given $H_{c2}(0) \sim 50 - 100$ T for oxypnictides [19]), shrinks the irreversible diamagnetic loop, while significantly increasing the paramagnetic component of $M(H)$. Further increase of H to 1.5T, practically eliminates the differ-

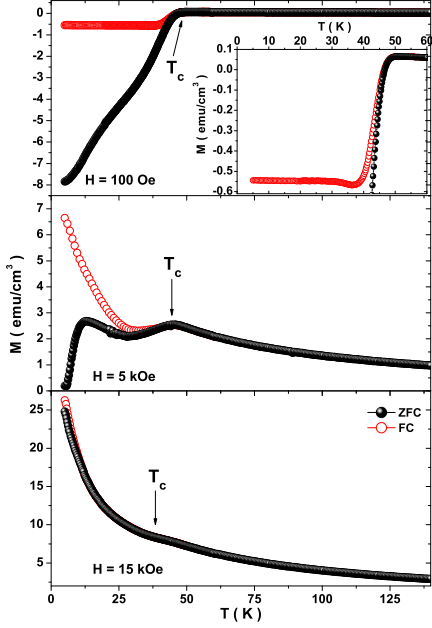


FIG. 1: ZFC (black full dots) and FC (red open dots) $M(T)$ at: 0.1, 5 and 15 kOe. Inset shows FC $M(T)$ at 0.1 kOe.

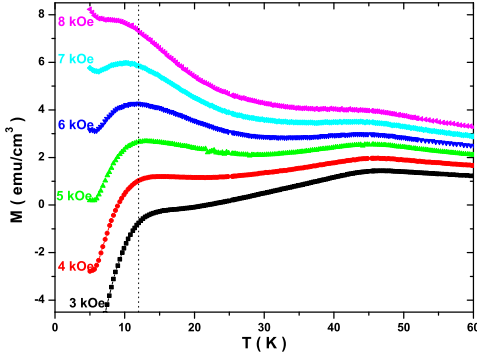


FIG. 2: ZFC magnetization at different fields. The dash line shows T_m extracted from the data in Fig.3.

ence between the ZFC and FC curves, both exhibiting a strong paramagnetic behavior. Fig. 2 shows in more detail how this field-induced superconducting to paramagnetic transition develops.

To gain a further insight into the nature of the paramagnetic signal not masked by superconductivity, $M(T, H)$ between 55 and 140 K was measured by a SQUID magnetometer. The results shown in Fig. 3 unambiguously indicate the AF Curie-Weiss behavior, $M^{-1} \propto T + T_m$ with $T_m \approx 11 - 12$ K being practically independent of H at $0 < B < 5$ T. This may indicate AF ordering at the Neel temperature $T_N \simeq T_m$, below the superconducting transition and a coexistence of superconductivity and antiferromagnetism in a variety of forms, for example, a quantum critical point as a function of doping. To see if this is indeed the case, we measured $M(T, H)$ below T_c at

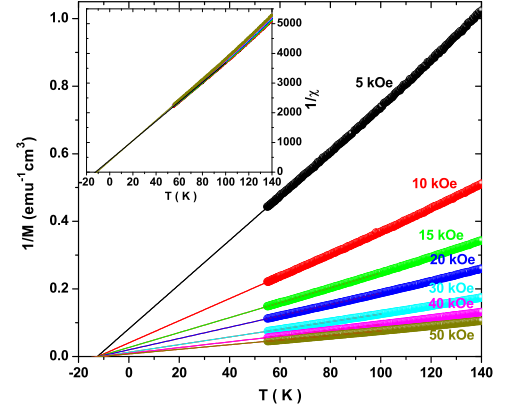


FIG. 3: The AF Curie-Weiss linear temperature dependence of $M^{-1}(T, H) \propto T + T_m$ in the normal state. The linear extrapolations defines $T_m \approx 11 - 12$ K. The inset shows the collapse of the inverse susceptibilities $\chi^{-1}(T, H) = H/M$ for different fields $0 < H < 5$ T onto a single straight line.

very high magnetic fields, which enabled us to suppress the irreversible magnetization due to pinned vortices and to probe $M(T, H)$ in the superconducting state at fields $H > T_N/\mu$ sufficient to destroy the global AF state.

Shown in Fig. 4a is the $M(H)$ loop at 4.2 K for the field perpendicular to the broader sample face. One can clearly see a superconducting hysteresis loop on top of a strongly paramagnetic, field-dependent background. Taking the mean value of the two branches of $m(B)$ as the paramagnetic magnetization, $M_p = (M_{\uparrow} + M_{\downarrow})/2$ plus the small reversible magnetization of the vortex lattice, we define the magnetization $\Delta M = M_{\uparrow} - M_{\downarrow}$ due to the critical state of pinned vortices. Using the Bean model, we estimate the critical current density $J_c(4.2K) \sim 10$ kA/cm² at self field. $M(H)$ in Fig. 4a increases with field and tends to level off at higher H . To probe the region of higher fields, $M(H, T)$ was measured in a 33T resistive magnet. The results presented in Fig. 4b, show that $M(4.2K, H)$ does saturate, while $M(T, H)$ at higher temperatures increases much slower as H increases. The width of superconducting loop decreases as T and H increase, consistent with the usual behavior of $J_c(H, T)$.

To interpret our data we used the mean-field AF theory in which two magnetic sublattices with the magnetizations M_1 and M_2 are controlled by the molecular fields $H_1 = H + aM_1 - bM_2$ and $H_2 = H + aM_2 - bM_1$, where a and b quantify the exchange interaction with nearest neighbors of the same spin sublattice (a) and the sublattice with the opposite spins (b) [21]. The self-consistency equations, $2M_i = M_0 B_J(\mu H_i/T)$, $i = 1, 2$ determine the total magnetization, $M(T, H) = M_1 + M_2$, and the AF order parameter $L(T, H) = M_1 - M_2$ where $M_0 = n\mu$, μ is an elementary magnetic moment, n is their total density, $B_J(z) = [(2J + 1)/2J] \coth[(2J + 1)z/2J] - (1/2J) \coth(z/2J)$ is the Brillouin function, and

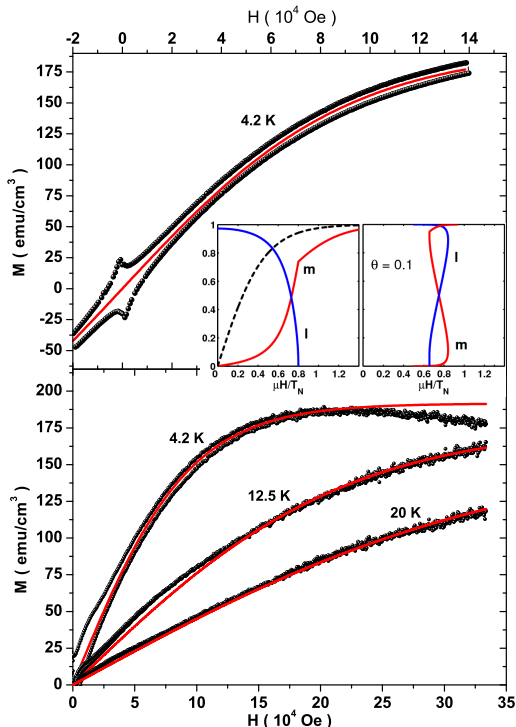


FIG. 4: (a) Low-field $M(H)$ loop measured by VSM at 4.2 K. The red line shows $M = M_0 \tanh(\mu B/T)$ with $B = H + 4\pi M$, $M_0 = \mu n$ for $\mu = 0.69\mu_B$, $M_0 V = 0.135$ emu and $n = 3 \times 10^{22}$ cm^{-3} . Inset shows $m(H)$ and $l(H)$ calculated from Eqs. (2)-(6) for $\gamma = 0.5$, and $m = \tanh(h)$ (dashed line). Here the left panel shows the second order transition for $\theta = 5/11$, and the right panel shows the first order metamagnetic transition for $\theta = 0.1$. (b) High-field $M(H)$ loops at different T. The red lines show $M = M_0 \tanh(\mu B/T)$ with $\mu = 0.67\mu_B$, $M_0 V = 0.133$ emu, $n = 3.1 \times 10^{22}$ cm^{-3} (4.2K); $\mu = 0.85\mu_B$, $M_0 V = 0.123$ emu, $n = 2.25 \times 10^{22}$ cm^{-3} (12.5 K); $\mu = 0.85\mu_B$, $M_0 V = 0.112$ emu, $n = 2.05 \times 10^{22}$ cm^{-3} (20 K).

J is the maximum magnetic quantum number. Expansion of $B_J(\mu B_i/T)$ in $\mu H_i/T$ at $T \gg T_N$ gives the linear temperature dependence for $1/\chi(T, H) = H/M$:

$$\frac{\chi(T_*)}{\chi(T, H)} = \frac{T + T_m(H)}{T_* + T_m(H)}, \quad (1)$$

Here $T_m = (b-a)M_0(J+1)/6J$, $T_* = 2T_m$, $T_m(B) = [1 - c_J(\mu H/T)^2]T_m$, $c_J = (2J^2 + 2J + 1)/10J^2$, and $\chi(T_*) = 9JT_m/(J+1)\mu M_0$, $T_m = \gamma T_N$ where $\gamma = (b-a)/(b+a) < 1$. Eq. (1) describes the data in Fig. 3 well, allowing us to estimate the density n of magnetic moments μ , which can provide the observed χ . Taking $\chi_0 = n\mu^2/3T_m = 1/395$ from the inset of Fig. 3, $T_m = 12$ K, and $\mu = 3.62\mu_B$ for Nd^{3+} [21], we obtain $n = 3T_m\chi_0/\mu^2 \simeq 1.5 \times 10^{22}$ cm^{-3} , close to the density of Nd atoms. Since the strong paramagnetism above T_c is only consistent with an atomic density of magnetic moments $\mu \simeq 3 - 4\mu_B$, Fe^{3+} with much smaller $\mu \simeq 0.25 - 0.35\mu_B$ [2, 3] can only add a few percent to $\chi \propto \mu^2$. The crystalline field

splits the degenerate orbital term of Nd^{3+} [21, 22] into terms with spin moments μ smaller than μ of the free Nd^{3+} but with n greater than the atomic density.

We consider breakdown of AF by strong fields using a simple model, in which only spin degrees of freedom contribute to M , so the mean-field equations, $2M_1 = M_0 \tanh(\mu H_1/T)$ and $2M_2 = M_0 \tanh(\mu H_2/T)$ can be reduced to the following parametric equations

$$z = \cosh^{-1}[(2/\theta s) \sinh s - \cosh s], \quad (2)$$

$$m = \sinh z / (\cosh z + \cosh s), \quad (3)$$

$$l = \theta s/2, \quad h = z\theta/2 + \gamma x, \quad (4)$$

which define the dimensionless magnetization $m = M/M_0$ and the order parameter $l = L/M_0$ as functions of the dimensionless field $h = \mu H/T_N$ and temperature $\theta = T/T_N$. Here the parameter s runs from 0 to $2/\theta$, and $T_N = M_0(b+a)/2$. For $T < T_N$, the AF order parameter $L(H, T)$ decreases as H increases, vanishing at the second order phase transition field $H = H_p$:

$$H_p = [\gamma\sqrt{1-\theta} + \theta \cosh^{-1}(1/\sqrt{\theta})]T_N/\mu, \quad (5)$$

at which $M(H_p) = M_0\sqrt{1-\theta}$. For $H > H_p$, the magnetization in the paramagnetic phase is described by

$$m = \tanh[(h - \gamma x)/\theta] \quad (6)$$

Shown in the inset of Fig. 4 are $m(h)$ and $l(h)$ curves calculated from Eqs. (2)-(6) for high ($\theta = 5/11$) and low ($\theta = 0.1$) temperatures. At high temperatures $m(h)$ has an upward curvature at $H < H_p$ and the downward curvature above the second order phase transition field H_p at which $L(H)$ vanishes. At low temperatures, $m(h)$ and $l(h)$ become multivalued, indicating hysteretic first order metamagnetic transitions due to spin flip in the sublattice with m antiparallel to H .

One can immediately see a very different behavior of the mean-field $M(H)$ as compared to the observed $M_p(H)$. Indeed, all $M_p(H)$ curves exhibit downward curvatures and can be described well by the Brillouin function $M = M_0 \tanh(\mu H/T)$ with $M_0 = \mu n$, $\mu = (0.67 - 0.85)\mu_B$ and $n = (2 - 3) \times 10^{22}$ cm^{-3} (the full set of fit parameters is given in the caption of Fig. 4). These values of n are about 2 times higher than the density of Nd^{3+} in $\text{Nd}(\text{O},\text{F})\text{FeAs}$, which may indicate splitting of the $^4I_{9/2}$ ground term of Nd^{3+} into different spin levels. Yet $M_p(H)$ shows no long-range AF behavior below T_c , otherwise $m(H)$ would be significantly depressed at $H < H_p$, as depicted in the inset of Fig. 4. For example, if $T_N = 11\text{K}$, $\theta = 5/11$, $\mu = 0.8\mu_B$, and $\gamma = 0.5$, Eq. (5) yields the field $H_p \simeq 16\text{T}$ required to destroy the AF state. However, $M(H)$ in Fig. 4a exhibits neither the downward curvature nor metamagnetic transitions characteristic of the mean-field behavior at $H < H_p$, while the data in Fig. 4b exhibit no sign of this behavior on a greater magnetic field scale either. Therefore,

the long-range AF ordering below T_c is inconsistent with our data, in agreement with the conclusion drawn from neutron scattering measurements on La(O,F)AsF [2]. At the same time, the Brillouin function for noninteracting spins gives a good description of the observed behavior of $M(T, H)$ at $T < T_c$, particularly the saturation of $M(H)$ at higher H and decreasing the low-field slope of $M(T) \sim \mu^2 n H / T$ as T increases.

In polycrystals $M(T, H)$ should be averaged with respect to easy magnetization directions in randomly oriented crystallites. For a uniaxial magnetic anisotropy and uniform distribution of easy magnetization axes inclined by angles θ with respect to H , we have, $\bar{M} = \int_0^{\pi/2} M(\mu H \cos \theta / T) \cos \theta \sin \theta d\theta$ and $\chi = \chi_{\parallel} / 3 + 2\chi_{\perp} / 3$, where $\chi_{\parallel} = 2(1 - l^2)T_N / (a + b)[T + (1 - l^2)\gamma T_N]$ and $\chi_{\perp} = 1/b$. If the in-plane AF structure is present, one can expect suppression of the AF state and local metamagnetic transitions at lower T in the grains for which the in-plane field component $H \cos \theta$ exceeds H_p . Also out-of-plane spin-flip transitions may occur if the perpendicular field component $H \sin \theta$ exceeds $H_c = [2K / (\chi_{\perp} - \chi_{\parallel})]^{1/2}$, where K is the energy of magnetic anisotropy [21].

Now we discuss possible mechanisms behind the observed effects. The first candidate would be paramagnetism of Nd^{3+} ions whose exchange interaction is mediated by conducting electrons on the AsFe planes. As follows from Fig. 3, this interaction could provide the AF ordering in the normal state below $T_N = T_m / \gamma \sim 10 - 20\text{K}$ with $\gamma < 1$. However, the superconducting transition in the AsFe planes sandwiched between Nd(O,F) planes occurs at temperatures $T_c > T_N$ effectively cutting off the 3D RKKY interaction [23] of Nd ions from different planes and reducing T_N of the 2D XY moments of single Nd planes to zero. This may explain why the simplest Brillouin function describes our data so well. Since the paramagnetic signal is so strong that the density of the magnetic moments $n \sim (2 - 3) \times 10^{22} \text{ cm}^{-3}$ is comparable to the atomic density of Nd ions, we can rule out that the behavior of $M(T, H)$ is controlled by a small fraction of partially reacted magnetic second phases.

Our high field measurements enable us to set a lower limit for T_N of AF ordered Fe^{3+} sublattice. In this case the longitudinal susceptibility χ_{\parallel} at low T and $H < H_p$ is dominated by paramagnetism of Nd ions. However, as H becomes of the order of T_N / μ the AF magnetization of the Fe sublattice becomes strongly nonlinear, exhibiting metamagnetic or spin flop transitions, which would manifest themselves in jumps on $m(H)$ curves. Since no sign of such behavior has been observed up to $H_{max} = 33 \text{ T}$, the long-range AF order can only be consistent with our results if H_p given by Eq. (5) is greater than H_{max} , thus $T_N \gg T_p$, where $H_p(T_p) = H_{max}$. For $H_{max} = 33\text{T}$, $\mu = 0.35\mu_B$ [6, 7], $T = 20 \text{ K}$ and $\gamma = 0.5$, Eq. (5) gives $T_p \approx 21 \text{ K}$. However, T_N much greater than 21K would be hard to reconcile with the Curie-Weiss behavior in Fig. 3 with $T_m = \gamma T_N \approx 11 - 12 \text{ K}$, unless $\gamma \ll 1$.

Another possibility is a spin-glass state for which $m(H)$ generally exhibits the behavior similar to that in the left inset in Fig. 4 with a broadened cusp around H_p and possible kinks and hysteretic jumps [24]. Yet the behavior resembling that of $M(H, 4.2\text{K})$ has also been observed on some metallic spin glasses, although on a much smaller field scale [24]. Such a spin glass state could result from Nd ions and weakly coupled AF clusters of Fe^{3+} , so that $\bar{M} = M_0 \int_0^{\infty} F(\mu_i) \tanh(\mu_i H / T) d\mu_i$ where the distribution function $F(\mu_i)$ can be expressed in terms of the distribution function of cluster sizes. This mechanism may also contribute to the fractional moment $\mu = \int_0^{\infty} \mu_i F(\mu_i) d\mu_i$ obtained from the fit in Fig. 4. AF clusters of Fe^{3+} around oxygen vacancies were revealed by the Mossbauer spectroscopy of $\text{SmO}_{1-x}\text{F}_x\text{FeAs}$ [9].

In conclusion, doped Nd(O,F)FeAs can be regarded as a paramagnetic superconductor in which magnetization is dominated by the Curie-Weiss paramagnetism of the rare earth ions. Our high field magnetization measurements have shown no long-range antiferromagnetic order below T_c despite noticeable AF correlations above T_c .

The work at NHMFL was supported by the NSF grant DMR-0084173 with support from the state of Florida and AFOSR. CT is grateful to Eun Sang Choi for help with high-field measurements.

-
- [1] Y. Kamihara, T. Watanabe, M. Hirano, and H. Hosono. J. Am. Chem. Soc. **130**, 3296 (2008).
 - [2] C. de la Cruz *et al.*, arXiv:0804.0795v1.
 - [3] M.A. McGure *et al.*, arXiv:0804.0796v1.
 - [4] A.J. Drew *et al.*, arXiv:0805.1042v1.
 - [5] R. Khasanov *et al.* arXiv:0805.1923v1.
 - [6] K. Ahilan *et al.*, arXiv:0804.4026v1.
 - [7] Y. Nakai *et al.*, arXiv:0804.4765v1.
 - [8] S. Kiato *et al.*, arXiv:0805.0041.
 - [9] I. Felner *et al.*, ArXiv: 0805.2794
 - [10] G.F. Chen *et al.*, arXiv:0803.3790v2.
 - [11] H.-H. Wen *et al.*, Europhys. Lett. **80**, 17009 (2008).
 - [12] A.S. Sefat *et al.*, Phys. Rev. B **77**, 174503 (2008).
 - [13] Z.A. Ren *et al.* Europhys. Lett. **82**, 57002 (2008).
 - [14] D.J. Singh, D.J. and M.H. Du. arXiv:0803.0429v1.
 - [15] I.I. Mazin *et al.* arXiv:0803.2740v1.
 - [16] C. Cao, P.J. Hirschfeld, H-P. Cheng. arXiv:0803.3236.
 - [17] J. Dong *et al.* arXiv:0803.3426v1.
 - [18] S. Ishibashi, K. Terakura, H. Hosono. J. Phys. Soc. Jap. **77**, 053709 (2008).
 - [19] F. Hunte *et al.*, Nature (2008).
 - [20] X. Zhu *et al.* arXiv:0803.1288v1.
 - [21] K.H.J. Buschow and F.R. de Boer *Physics of Magnetism and Magnetic Materials* (Kluwer, New York, Boston, Dordrecht, London, Moscow, 2004).
 - [22] J. Wu, P. Phillips, A.H. Castro Nero. arXiv:0805.2167v1.
 - [23] A.V. Balatsky, I. Vekhter, and J.-X. Zhu, Rev. Mod. Phys. **78**, 373 (2006).
 - [24] K. Binder and A.P. Young, Rev. Mod. Phys. **58**, 801 (1986).